DOI: 10.2478/rjti-2024-0003

ROMANIAN JOURNAL
OF TRANSPORT INFRASTRUCTURE

MICROMECHANICAL MODELING FOR ANALYSIS OF SHEAR WAVE PROPAGATION IN GRANULAR MATERIAL

Said DERBANE*, Department of Civil Engineering, LMGHU Laboratory, University of 20 August 1955 Skikda, BP 26, 21000, Skikda, Algeria, *corresponding author's e-mail: derbane_said@yahoo.fr
Mouloud MANSOURI, Civil Engineering Research Laboratory of Setif (LRGCS), Department of Civil Engineering, Ferhat Abbas University of Setif 1, Setif 19000, Algeria
Salah MESSAST, Department of Civil Engineering, LMGHU Laboratory, University of 20 August 1955 Skikda, BP 26, 21000, Skikda, Algeria.

Abstract

This paper presents a numerical study of shear wave propagation in a vertical sand profile through micromechanical modeling. For this purpose, 2D modeling by the Discrete Element Method (DEM), is carried out. The DEM model is based on molecular dynamics with the use of circular elements. The intergranular normal forces at contacts are calculated through a linear viscoelastic law, while the tangential forces are calculated through a perfectly plastic viscoelastic model. Rolling friction is incorporated to account for the damping of the grains rolling motion. Different boundary conditions of the profile have been implemented: a bedrock at the base, a free surface at the top, and periodic boundaries in the horizontal direction. The sand deposit is subjected to a harmonic excitation at the base. The simulations carried out have well reproduced the elastic and damping features relative to shear wave propagation in a vertical soil deposit. The excitation frequency is varied to better understand the phenomenon of wave propagation in granular medium. The conducted simulations highlighted a number of features of soil deposits response subjected to harmonic excitation at the base, including the movement amplification, the resonance phenomenon and the limitation of the displacement at the resonance. The micromechanical analysis showed that the intergranular slips increase with increasing the involved strain level. An inverse analysis is performed to determine a continuum-damped linear elastic model, whose response is similar to that of the discrete-element model. This analysis showed that the wave propagation velocity of the equivalent continuum model decreases with increasing excitation frequency. This finding could be attributed the decrease of shear modulus of the granular material as the deformation level increases.

Keywords: Micromechanical, Granular material, Discrete Element Method, Shear wave.

1. INTRODUCTION

It is generally accepted that the seismic motion felt at a ground surface is induced by tectonic plates and transmitted to the surface by the deposit of soil overlying these plates. Consequently, the properties of the soil traversed have a significant effect on the transmitted motion. Models commonly used to characterize this transmission of movement assume the continuity of the soil material. While this assumption seems effective under certain conditions related to the motion transmitted and the type of soil traversed, it becomes increasingly ineffective when dealing with naturally discontinuous soils such as sand, and when the motion is strong. Under these conditions, the discrete element method may be more appropriate, since it inherently considers material discontinuities and intergranular slippage that occur at high amplitudes of motion.

DEM is a numerical technique that treats individual particles as separate entities in order to mimic the behavior of granular materials. This makes it possible to record the intricate interactions between particles, which are crucial for comprehending how granular soils behave. Through the study of natural processes like the liquefaction of sands under Rayleigh waves, this method has recently demonstrated its value in the field of geotechnics [1], [2], [3]. Conversely, in the realm of rail transport, Guo et al. [4] and Kumar et al. [5] have employed DEM to verify the stability of the ballasts under cyclical loads. The shear modulus and damping of granular materials for low frequencies, have been characterized using wave propagation modeling using digital emission modeling [6]. Sadd et al. investigated the factors affecting a group of grains with the same diameter's attenuation of wave amplitudes [7]. In a cubical cell setup, O'Donovan et al. used DEM to model the propagation of waves through a granular material [8]. Sakamura and Komaki conducted simulations of shock-induced load transfer processes in granular medium [9]. Shear wave propagation in granular assemblies has been modeled by Ning et al [10], who have also examined the impact of particle size and elastic characteristics on wave velocity. Tang and Yang examined how a granular material's grain structure affected the way waves propagated through it [11]. Peters and Muthuswamy investigated the impact of force chains on wave propagation in cohesionless granular packing [12]. In cohesionless granular materials, the primary propagation path of a dynamic load was identified using the dynamic force chains by Longlong and Shunhua Zhou [13] and Longlong et al [14]. The issue of force chain stability is examined by Charles and Campbell [15].

In the present work, a 2D numerical study of the shear wave propagation in a vertical sand profile is performed. For this objective, a model of discrete elements is developed, numerical simulations have been carried out to study the response of the profile to movements with different excitation frequencies and thickness. The analysis of the propagation is done in time domain the nonlinear behavior of the material is inherently taken into account in this model. This numerical approach allows us to understand a number of essential characteristics of wave propagation, including motion amplification, excitation frequency, resonance frequency, layer height and confining pressure.

2. DISCRETE ELEMENT METHODS FOR GRANULAR MATERIALS MODELING

The molecular dynamics technique serves as the foundation for the discrete element model used in this work. It uses independent parts to simulate the granular material at the micromechanical scale. Each grain of the material interacts with its neighbors at the contact points, creating contact pressures between them. According to Mansouri and El Youssoufi [16] and Pöschel and Schwager [17], the relative motions of the grains that are thought of as rigid entities are primarily responsible for the medium's global deformation. In order to optimize the modeling time, it is crucial to select grains with a basic shape [11]. Spheres are utilized for three-dimensional modeling and discs for two-dimensional modeling due to their simplicity in modeling.

2.1. Equations of motion

The parameter that determines the overall behavior of the medium is the movement of the grains, which obeys Newton's second law (Equation 1), from which the accelerations of the grains are obtained. These equations are constructed with consideration for all external forces, such as contact and gravitational forces, and their integration must be done gradually with sufficiently short time increments. As a result, discretizing time in relatively short increments is required in order to effectively forecast locations, velocities, and accelerations. A first prediction step using the acceleration at the beginning of the time step and a second correction step using the acceleration at the conclusion of the time step are used to derive the development of grain displacements from one-time step to the next. Positions and velocities are adjusted in accordance with changes in acceleration during the course of the time step. The grain trajectory was numerically calculated using two methods: the "Velocity-Verlet" technique and Gear's "predictor-corrector" algorithm.

$$\begin{cases} m_i \ddot{\vec{x}}_i = \sum_j \vec{F}_{ij}^{contact} + m_i \vec{g} \\ I_i \ddot{\vec{\varphi}}_i = \sum_j \vec{M}_{ij}^{contact} \end{cases} \tag{1}$$

With : $\ddot{\vec{x}}_i$ and $\ddot{\vec{\varphi}}_i$: The translational and rotational accelerations of the grains.
m_i and I_i : The mass and the moment of inertia respectively.
$\vec{F}_{ij}^{contact}$: The interaction force applied by a grain j in contact with grain i.
$\vec{g}$: The acceleration due to gravity.
$\vec{M}_{ij}^{contact}$: The moments caused with respect to the center of gravity of grain i by the contact forces $\vec{F}_{ij}^{contact}$.

2.2. Law of interaction between grains

2.2.1. Contact forces

The contact force is the normal and repulsive part of the interaction force. It is acknowledged that the definition we might use is the product of an elastic and a dissipation force. Usually, the dissipation is linked to the grains' loss of kinetic energy or, less frequently, the contact's flexibility. A simplified decomposition is used to study contact forces; a normal component $\vec{F}_n$ and a tangential component $\vec{F}_s$ included in the plane tangent to the grain at the point of contact [20]. The evaluation of interaction forces is usually done according to an appropriate interaction law. The orientation of the tangential force $\vec{F}_s$ is given by the direction of the relative tangential velocity between the two grains at the time of contact.

The Normal Contact Force is presented by a viscoelastic model (Figure 1.a), $\vec{F}_n$ is given by Heitz [21]:

$$\vec{F}_n = (-k_n D_n - v_n V_n).\vec{n} \tag{2}$$

Where: k_n: The elastic constant.
v_n: The viscous damping constant.
V_n : The normal velocity.

The normal distance between two grains i and j denoted D_n is defined geometrically by:

$$D_n = \left\| \vec{x}_j - \vec{x}_i \right\| - r_i - r_j \tag{3}$$

In which r_i and r_j are the radius of grains i and j.

It should be noted that the elastic stiffness and the viscous damping (k_n and ν_n) are chosen in a way to correctly model the behavior of the material. In fact, k_n must be large enough to avoid a substantial overlap which affects the overall behavior, while ν_n controls the damping in the material, it is calculated from the coefficient of restitution ε_n which represents the ratio between the separation velocity (rebound velocity) V_{ns} and the contact initiation velocity (impact velocity) V_{n0}. The value of this coefficient is naturally between 0 and 1. Thus, the viscous damping coefficient ν_n is obtained as a function of the restitution coefficient according to equation [16]:

$$\nu_n = -\frac{2\log(\varepsilon_n)\sqrt{k_n m_{eff}}}{\sqrt{\pi^2 + (\ln \varepsilon_n)^2}} \tag{4}$$

$$m_{eff} = \frac{m_i m_j}{(m_i + m_j)} \tag{5}$$

With : m_i and m_j being the masses of the two grains in contact.

The tangential contact force is presented by a viscoelastic model with bearing (Figure 1.b) (Semblat and Luong, 1998), $\vec{F_s}$ is given by:

$$\vec{F_s} = min(k_s D_s + v_s V_s,\ \mu_d F_n)\vec{s} \tag{6}$$

Where k_s is the tangential stiffness, v_s the viscous damping coefficient, μ_d is the inter-particle coefficient of friction, D_s is the grain deformation due to shear force. V_s is the tangential velocity of grain j with respect to grain i.

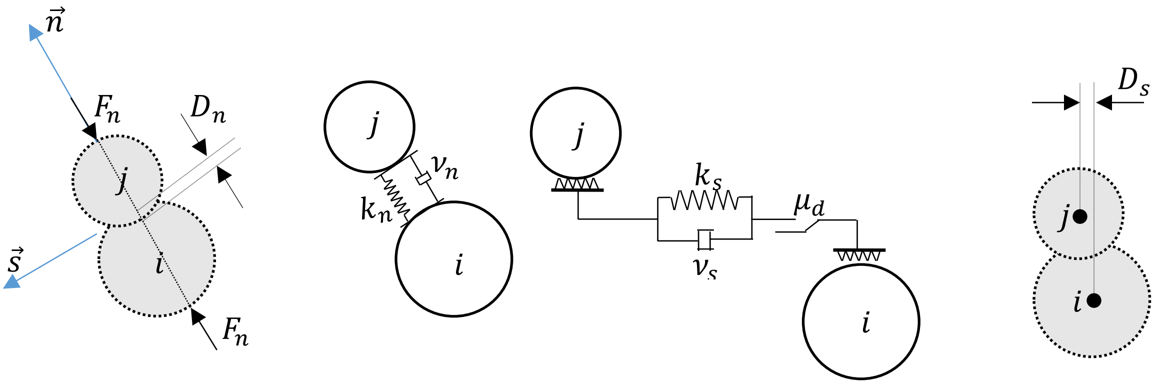

Figure 1. Normal force (a) and shear force (b) between grains

2.2.2 Contact duration

The duration of a contact t_c is half the natural period of the oscillator and can be expressed as:

$$t_c = \pi\sqrt{\frac{m_{eff}}{k_n}} \tag{7}$$

This contact duration t_c is of practical importance. Indeed, the integration of the equations of motion is only stable if the integration time step Δt is sufficiently small compared to t_c, in other words, the evolution of the contact should be well described. Otherwise, calculation instabilities may occur due to late detection or even non-detection of contacts. To avoid these instabilities, it is common to discretize the duration of the contact t_c at least in ten time steps [23]:

$$\Delta t_{max} \approx 0.1\pi\sqrt{\frac{m}{k_n}} \tag{8}$$

Where : m is the smallest effective mass in the system.

3. WAVE PROPAGATION MODELING

The current work involves 2D modeling of shear wave propagation in a vertical sand profile. This model, which is implemented in C++ code, is based on discrete element modeling.

The grains of the sand profile are pluviated under gravity to form a dense deposit. Various boundary conditions are taken into consideration: a chain of grains is introduced onto this bedrock, through which a controlled horizontal displacement is applied; a weighing chain of grains is introduced at the surface of the deposit; in order to study the confinement pressure of the soil layer, the interactions between the grains of the chain and the deposit grains are treated with the same interaction models used in the interactions of the deposit grains; periodic boundaries have been introduced to represent an infinite profile in the horizontal direction; the upper surface is considered free, and the profile is delimited and supported at the base by a wall, which is considered a bedrock.

A harmonic displacement with specific amplitude and frequency is applied to the grain chain at the bottom of the profile in order to investigate the shear wave propagation in the profile. The deposit of granular material is divided into a predetermined number of layers, and when the profile is excited, the average displacements in each layer are recorded.

4. RESULTS OF NUMERICAL SIMULATIONS AND DISCUSSION

4.1. Model Parameters

Figure 2 shows the sand profile model subjected to a base excitation; the different boundary conditions are indicated.

The properties of the grains as well as the micromechanical parameters used in the computation of the contact forces between the grains are presented in Table 1.

Table 1. Simulation parameters.

Parameters	**Value**
Grains number	5000
Grain radius r_i	$1.00\text{x}10^{-3}$ to $2.00\text{x}10^{-3}$
Density G_s	2600 kg/m^3
Contact normal stiffness k_n	$1.2\ \text{x}10^{6} N/m$
Contact shear stiffness k_s	$9.6\text{x}10^{5} N/m$
Inter-particle friction coefficient μ	0.5

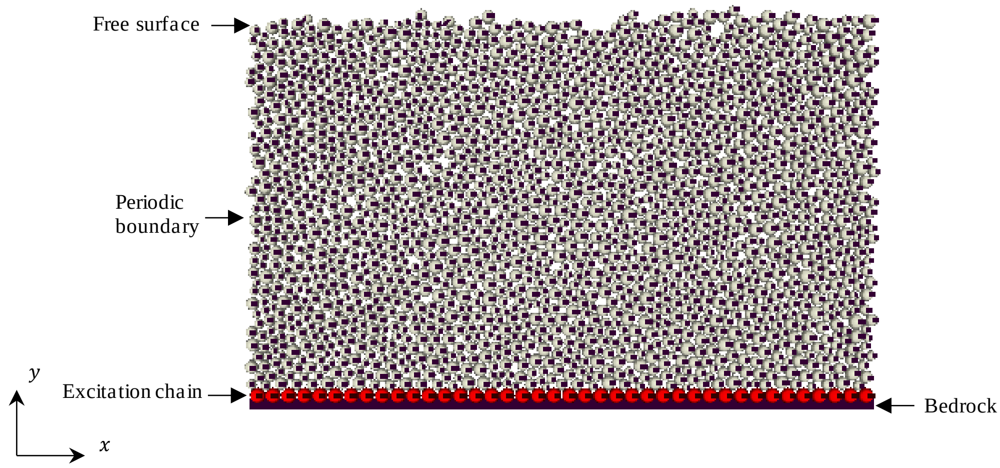

Figure 2. Sand profile and boundary condition

This sand profile is built by pluviating grains under gravity, and after stabilization of a number of 5000 grains throughout a 1.4-meter-wide area, the obtained deposit's height is about 0.74 m. This deposit is subjected to a harmonic excitation at its base $u(t) = A_0 \sin(\omega t)$ with $A_0 = 2x10^{-4}m$ and $\omega = 20\, rad/s$. The dynamic amplification factor (R_d) at the top layer of the deposit is defined with :

$$R_d = \frac{A}{A_0} \tag{9}$$

Where : A denotes the displacement amplitude at the top layer; A_0 is the displacement amplitude at the bedrock i.e. the base excitation.

4. ANALYSIS OF SHEAR WAVE PROPAGATION IN THE SAND PROFILE

In order to avoid perturbations due to the transient response of the profile, the amplitude of the excitation is gradually increased during 4.5 seconds to reach a maximum of $2x10^{-4}\ m$, maintained for 6 seconds before gradually decreasing and reaching zero during 1.5 seconds (Figure 3a). By splitting the profile into ten sub-layers, horizontal motion propagation across the deposit is monitored. Every sub-layer's average displacement is tracked both during and after the excitation.

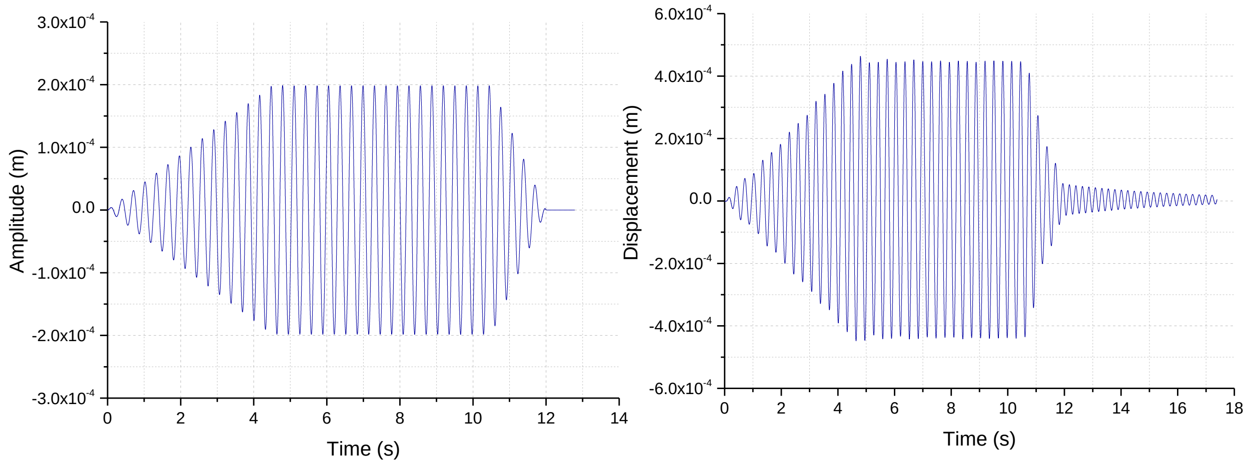

Figure 3. Variation of the excitation amplitude at the bedrock (a) and the response of profile (b)

Figure 3b presents the displacement at the top sub-layer during the excitation. It is evident that the introduced excitation movement is magnified at the top sub-layer by comparing the amplitude of the displacement at this layer with that of the excitation. This figure also demonstrates the damped vibration that the soil undergoes after the excitation is stopped, indicating elastic damped behavior in the deposit.

4.1. Highlighting the amplification of vibration

Figure 4 illustrates a part of the steady state response at the base, middle, and top layers $(7s \leq t \leq 8s)$.

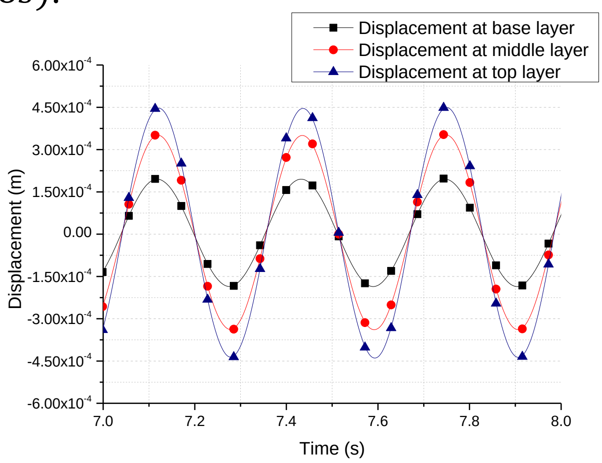

Figure 4. Variation of displacement from the base to the surface.

We observe that the motion from the base to the surface is gradually amplified. At the top sub-layer, the maximum displacement's amplification ratio (R_d) has a value of 2,28.
Figure 5 presents the evolution of the dynamic amplification factor versus the height with respect to the bedrock.

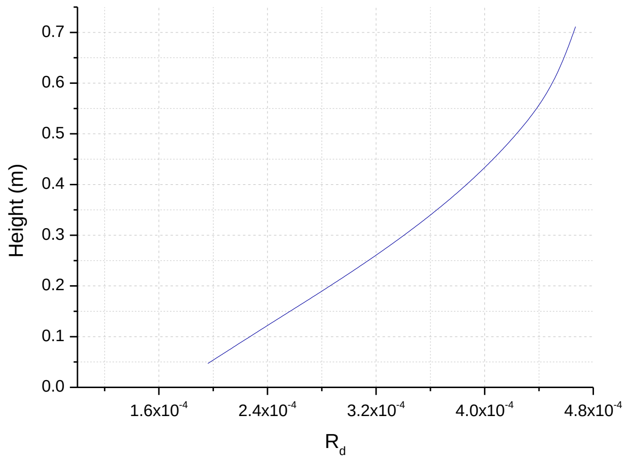

Figure 5. Variation of the dynamic amplification factor vs. the distance from the bedrock

This figure demonstrates the movement amplification from the bedrock to the top sub-layer. Additionally, it demonstrates that the excitation frequency being employed is less than the deposit's fundamental frequency, or first natural frequency.

4.2. Vibration properties at low amplitudes

Low vibration amplitudes are typically used to assess a deposit's fundamental frequency. The free vibration phase that results from stopping the excitation can be used to estimate the deposit's fundamental frequency for the current modeling. A magnification of the displacement history during this phase is displayed in Figure 6.

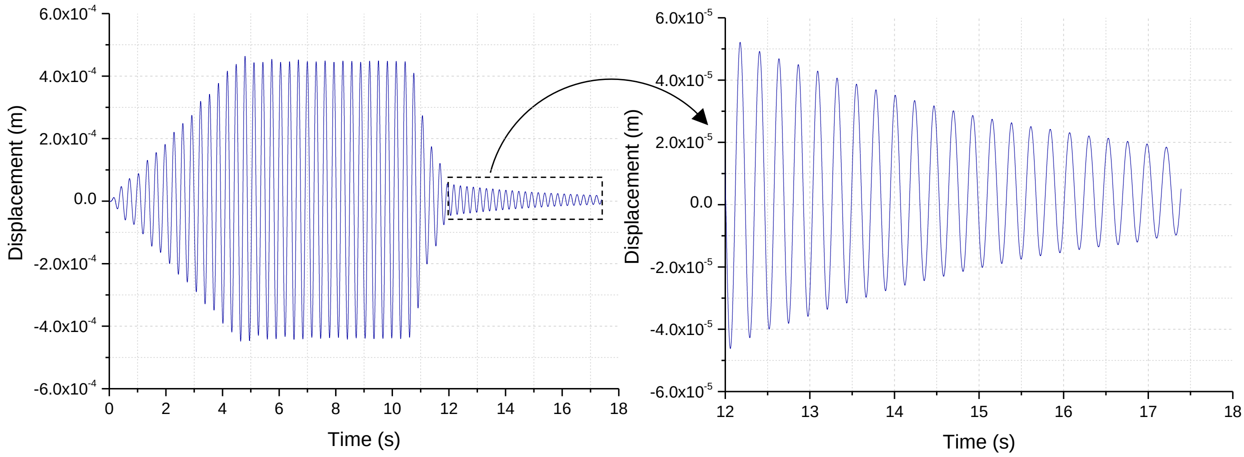

Figure 6. Top layer time history response at free vibration

The period of vibration estimated from the displacement plot is approximately $T = 0.2291s$. This period corresponds to a natural frequency $w = \frac{2\pi}{T} = 27{,}426\, rad/s$. From this frequency, it is possible to estimate the shear wave velocity in the deposit [24] using the formula $c = \frac{4H}{T} = 12.92 m/s$.

On the other hand, it is possible to estimate deposit's ratio for small vibration amplitudes using the logarithmic decrement expressed as [25]:

$$\xi = \frac{1}{\sqrt{1+(\frac{2\pi}{\delta})^2}} \tag{10}$$

With:

$$\delta = \ln(\frac{Y_{\max(i)}}{Y_{\max(i+1)}}) \tag{11}$$

In which δ is the logarithmic decrement, $Y_{\max(i)}$ and $Y_{\max(i+1)}$ are two successive pics in the free vibration.

The calculations based on the response curve of figure 4, give the damping ratio: $\xi = \frac{1}{\sqrt{1+(\frac{2\pi}{0{,}09754})^2}} = 1{,}55\%$.

These free vibrations with low amplitudes could be categorized as damped elastic vibrations. The resonant frequency should be somewhat lower given the low obtained damping value, but this is not the case for the fundamental frequency, which is approximately $27{,}426\, rad/s$.

4.3. Influence of the excitation frequency on the movement amplification

Different excitations with frequencies ranging from 10 to 30 rad/s were applied in order to examine the impact of excitation frequency on the deposit response and determine the first resonance frequency. The growth of the dynamic amplification factor at the top layer during the steady-state phase is depicted in Figure 7.

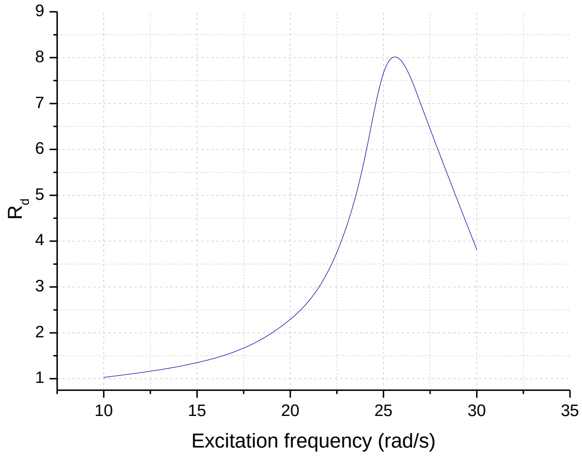

Figure 7. Dynamic Amplification Factor vs. excitation frequency

This figure demonstrates how R_d rises, reaches a peak, and then falls as the excitation frequency increases. The first resonance frequency, which is about $26 rad/s$, corresponds to the greatest value of the amplification. It should be emphasized that this is significantly lower than the fundamental frequency that was previously calculated using low-amplitude free vibration. This discrepancy is most likely caused by the shear modulus degradation at large vibration amplitudes.

4.4. Influence of the excitation frequency on the intergranular slips

During the excitation of the granular deposit, a movement of the grains is occurring. Slip movement occurs when the coulomb slip threshold is exceeded. This section deals with the variation of the global slip in the deposit as a function of the excitation frequency.

In order to study the influence of the excitation frequency on the cumulated intergranular slippage in the deposit, the deposit is subjected to a harmonic excitation with amplitude ($A_0 = 2x10^{-4}m$) and with different excitation frequencies (10rad/s, 15rad/s, 20rad/s, 23rad/s and 30rad/s).
Figure 8 presents the variation of the global slippage in the deposit with excitation frequency at steady state response ($4.5s \leq t \leq 10.5s$).

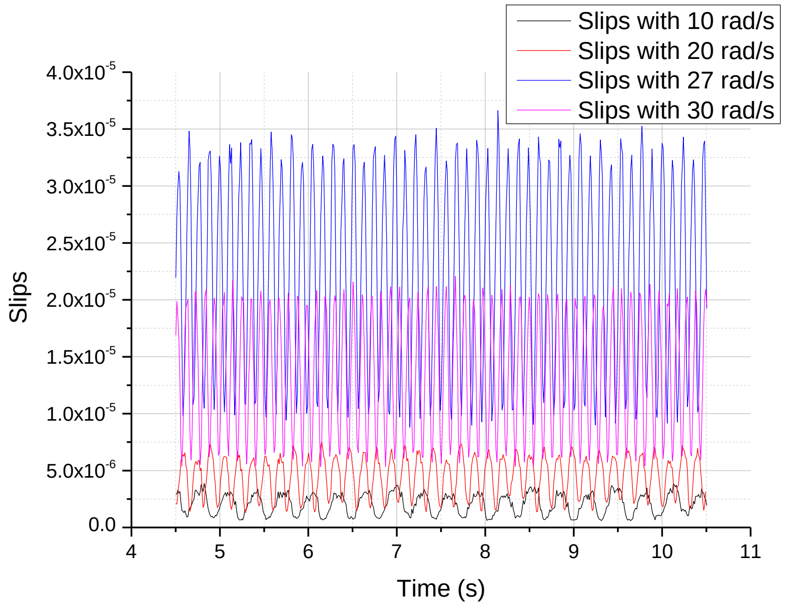

(a)

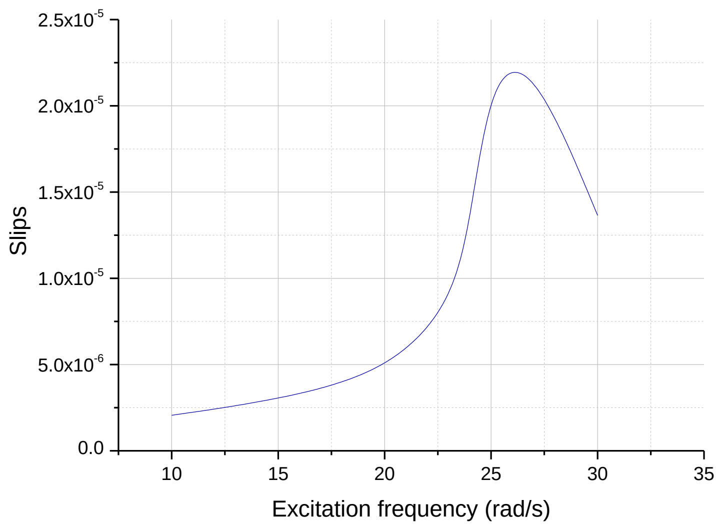

(b)

Figure 8. Global slippage. (a) Time history for different excitation frequencies, (b) Average global slippage vs. excitation frequency.

This figure demonstrates clearly that the overall slippage evolves in the same way as the dynamic amplification factor. Initially it increases with increasing frequency, reaching a peak at a frequency of around 27 rad/s, then decreases at higher frequencies. This evolution indicates that the average global slippage increases with the amplitude of the motion involved. Note that the frequency of 27 rad/s corresponds approximately to the resonance frequency as estimated in section 4.2.

4.5. Equivalent model with linear elastic damped continuum

In this section, we attempt to model the granular deposit by a continuum with damped linear elastic behavior. In this case, its response to harmonic excitation can be obtained analytically. Thus, an inverse analysis is performed to determine the material properties of the equivalent continuous medium, which give the same response as that of the discrete element numerical model. The analytical solution for the displacement of a hysteretically damped elastic deposit, subjected to harmonic excitation applied to its base, is given in reference [24] as follows:

$$\begin{aligned} \frac{A.u(z,t)}{u_0} = {} & \cosh(ph)\cos(qh)\cosh(pz)\cos(qz)\sin(\omega t) \\ & +\sinh(ph)\sin(qh)\sinh(pz)\sin(qz)\sin(\omega t) \\ & +\cosh(ph)\cos(qh)\sinh(pz)\sin(qz)\cos(\omega t) \\ & -\sinh(ph)\sin(qh)\cosh(pz)\operatorname{coc}(qz)\cos(\omega t) \end{aligned} \tag{12}$$

with:

$$A = cosh^2(ph) - sin^2(qh) \tag{13}$$

p and q are obtained from the equations $p^2 + q^2 = \frac{\omega^2/c^2}{1+4\xi^2}$ and $2pq = 2\xi\frac{\omega^2/c^2}{1+4\xi^2}$

And c is the wave velocity, ξ is the hysteretic damping ratio parameter and ω the circular excitation frequency.

In this solution, two material properties are involved: the wave propagation velocity, which depends on the stiffness and mass of the material, and the damping rate, which characterizes the energy lost during deformation. It's worth mentioning that the wave propagation velocity has a much more significant effect on response than the damping rate.

In order to compare the evolution of the depot response with frequency for the two methods, the numerical method (DEM) and the analytical solution (Eq. 12), we have calibrated the material parameter c (wave propagation velocity) in the analytical solution to provide a response similar to the numerical response. The damping ratio parameter (ξ) is set to an average value of 8%, since its effect on the response is small. The excitation amplitude is set to $A_0 = 2.10^{-5}m$, different excitation frequency are used (15 to 25 rad/s).

Figure 9 shows parts of the steady-state displacements $(6s \leq t \leq 8s)$ at the median layer, obtained by the DEM model with those of the analytical solution for the different frequencies. For each frequency, the wave propagation velocity that gives a response close to the numerical response is indicated below the graph.

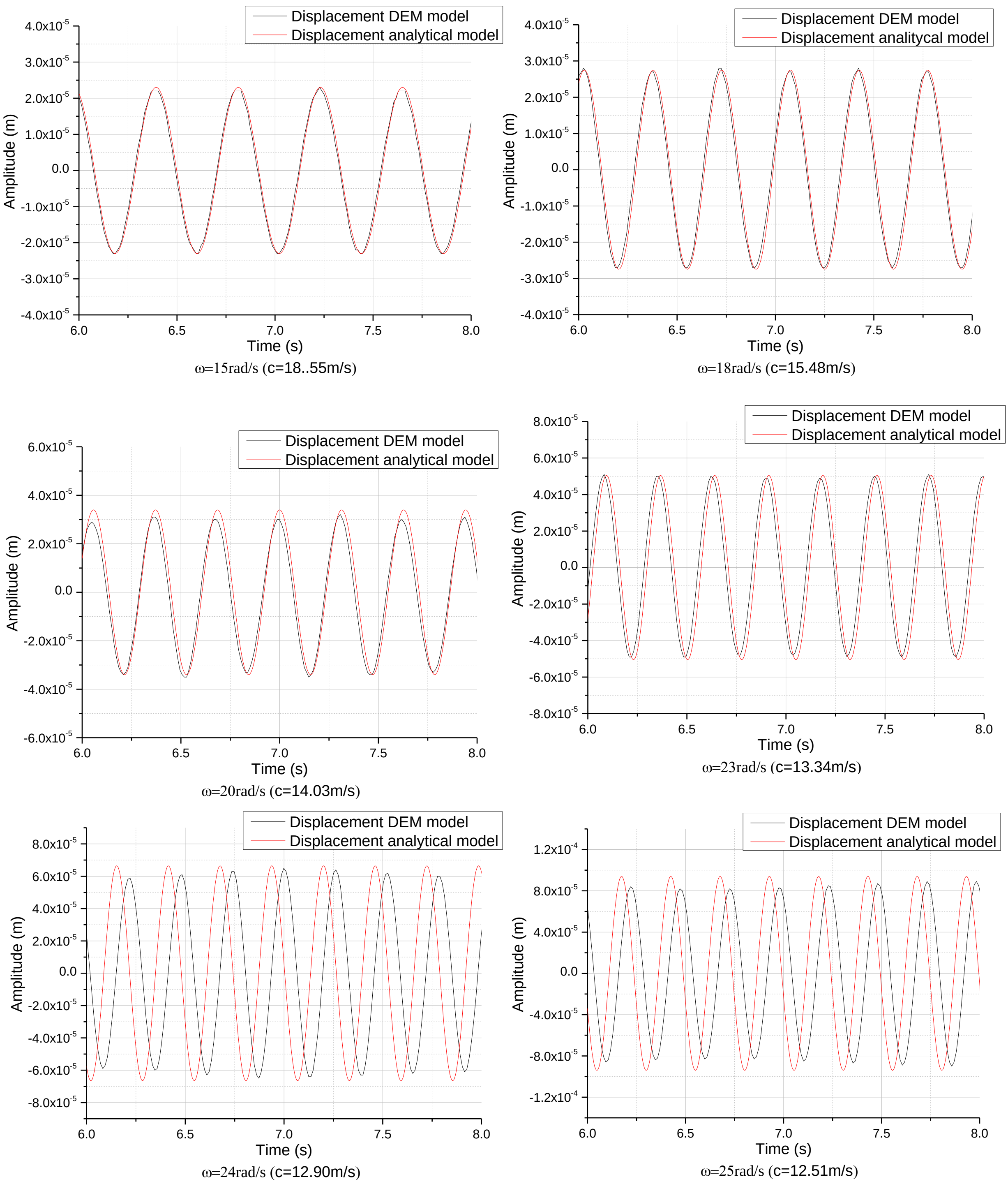

Figure 9. Displacements at the middle layer from the DEM model and analytical solution.

This figure shows a remarkable agreement between the two models. For the excitation frequencies of 15, 18, 20 and 23 *rad/s*, the displacements at the middle layer of the analytical solution are very close to the results of the DEM simulation with wave velocities of 18.55*m/s*, 15.48*m/s*, 14.03*m/s* and 13.34*m/s* respectively. On the other hand, for excitation frequencies of 24*rad/s* and 25*rad/s*, it becomes difficult to find wave propagation velocities for which the analytical solution matches the numerically obtained response**.** Indeed, at these frequencies which are close to resonance, irreversible displacements of the grains occur, and the analytical solution becomes incapable of modeling such behavior.

This comparison makes it possible to clearly conclude the limits of analytical methods in the analysis of wave propagation in soils, particularly when the excitation frequencies approach the resonance frequency.

Figure 10 shows the wave velocity versus frequency, which allows to reproduce the numerical response through the analytical solution.

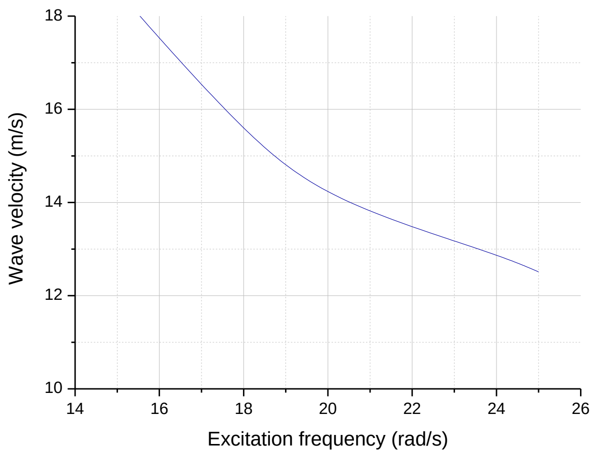

Figure 10. Wave velocity with excitation frequency

This figure indicates that the wave propagation velocity of the equivalent linear model decreases with excitation frequency, revealing that the effective shear modulus (stiffness property) of the numerical model decreases with frequency. This result is to be expected, since the strain level increases as the excitation frequency approaches the resonance frequency, and it is well established in classical soil dynamics that the shear modulus of granular soils decreases with increasing the strain level.

5. CONCLUSION

In this paper, discrete element modeling of shear wave propagation in a granular deposit is performed. The granular deposit is subjected to a harmonic displacement at its base, and its response is analyzed. The results obtained show that the model reproduces well the known features of the response of a soil deposit subjected to harmonic excitation at its base, namely the amplification of the motion which increases from bottom to top, the phenomenon of resonance when the excitation frequency approaches the fundamental frequency and the limitation of the amplitude during resonance. The micromechanical analysis, has shown that the intergranular slippage increases with the dynamic amplification. An inverse analysis is performed in order to determine a continuum damped linear elastic model, whose the response is similar to the response of the discrete element model. This analysis has shown that that the wave propagation propagation velocity of the equivalent continuum model is frequency dependant, it decreases with increasing excitation frequency. Such a result could be explained by the decrease of the shear modulus of the granular material when the strain level increases.

REFERENCES

[1] Jiang, M., Kamura, A. (2022), Numerical study on liquefaction characteristics of granular materials under Rayleigh-wave strain conditions using 3D DEM, soils and Foundations 62 (2022) 101176. https://doi.org/10.1016/j.sandf.2022.101176.

[2] Cui, J., Men, F., Wan, X., (2004), Soil liquefaction induced by Rayleigh wave. 13th World Conference on Earthquake Engineering.

[3] Nakase. H, Takeda. T, Oda. M, (1999), A simulation study on liquefaction using DEM. Proceedings of the 2nd International Conference on Earthquake Geotechnical Engineering, pp. 637–642.

[4] Guo, Y., Zhao, C., Markine, V., Jing, G., & Zhai, W. (2020). Calibration for discrete element modelling of railway ballast: A review. Transportation Geotechnics, 23, Article 100341. https://doi.org/10.1016/j.trgeo.2020.100341.

[5] Kumar, N., Suhr, B., Marschnig, S., Dietmaier, P., Marte, C., & Six, K. (2019). Micromechanical investigation of railway ballast behavior under cyclic loading in a box test using DEM: Effects of elastic layers and ballast types. Granular Matter, 21, 106. https://doi.org/10.1007/s10035-019-0956-9.

[6] Zamani, N., El Shamy, U. (2011), Analysis of wave propagation in dry granular soils using DEM simulations. Acta Geotechnica (2011) 6:167–182. https://doi.org/10.1007/s11440-011-0142-7.

[7] Sadd, MH., Adhikari, G., Cardoso, F. (2000), DEM simulation of wave propagation in granular materials, Powder Technology 109 Ž2000. 222–233. https://doi.org/10.1016/S0032-5910(99)00238-7.

[8] O'Donovan, J., Ibrahim, E., O'Sullivan, C., Hamlin, S., Muir Wood, D. & Marketos, G. (2016), Micromechanics of seismic wave propagation in granular materials, Granular Matter (2016) 18:56. https://doi.org/10.1007/s10035-015-0599-4.

[9] Sakamura, Y., Komaki, H. (2012), Numerical simulations of shock-induced load transfer processes in granular media using the discrete element method, Shock Waves (2012) 22:57–68. https://doi.org/10.1007/s00193-011-0347-6.

[10] Ning, Z., Khoubani, A., Evans, T.M. (2015), Shear wave propagation in granular assemblies, Computers and Geotechnics 69 (2015) 615–626. https://doi.org/10.1016/j.compgeo.2015.07.004.

[11] Tang, X., Yang, J. (2021), Wave propagation in granular material: What is the role of particle shape? Journal of the Mechanics and Physics of Solids 157 (2021) 104605. https://doi.org/10.1016/j.jmps.2021.104605.

[12] Peters, J. F., Muthuswamy, M. (2005), Characterization of force chains in granular materia, Phys. Rev. E 72, 041307. https://doi.org/10.1103/PhysRevE.72.041307

[13] Longlong Fu, Shunhua Zhou, Guo, P., Wang, S., & Luo, Z. (2019), Induced force chain anisotropy of cohesionless granular materials during biaxial compression, Granular Matter (2019) 21:52. https://doi.org/10.1007/s10035-019-0899-1.

[14] Longlong Fu, Shunhua Zhou, Zheng, Y., & Zhuang, L (2023), Characterizing dynamic load propagation in cohesionless granular packing using force chain, Particuology 81 (2023) 135e143. https://doi.org/10.1016/j.partic.2023.01.007.

[15] Charles S. Campbell (2003), A problem related to the stability of force chains, Granular Matter 5, 129–134. https://doi.org/10.1007/s10035-003-0138-6.

[16] Mansouri M, El Youssoufi MS (2016), Numerical simulation of the quicksand phenomenon by a 3D coupled Discrete Element - Lattice Boltzmann hydromechanical model, Int. J. Numer. Anal. Meth. Geomech. (2016). https://doi.org/10.1002/nag.2556.

[17] Pöschel T, Schwager T (2005). Computational Granular Dynamics - Models and Algorithms, Springer-Vrlag: Berlin Heidelberg, 2005.

[18] Richefeu. V, (2005), Approche par éléments discrets 3D du comportement de matériaux granulaires cohésifs faiblement contraints, thèse Université Montpellier II - Sciences et Techniques du Languedoc, 2005. Français. NNT: tel-00012112.

[19] Cundall PA, Strack ODL (1979). A discrete numerical model for granular assemblies. Géotechnique 29(1):47–65. https://doi.org/10.1680/geot.1979.29.1.47

[20] Delenne, J.Y., El Youssoufi, M.S., Cherblanc, F., Bénet, J.C. (2004), Int. J. Numer. Anal. Methods Geomech. 28, 1577 (2004).

[21] Heitz JF (1992) Wave propagation in non-linear medium. PhD Thesis, Grenoble University, France.

[22] Semblat JF, Luong MP (1998), Wave propagation through soils in centrifuge testing. J Earthquake Eng 2(10):147–171. https://doi.org/10.1080/13632469809350317.

[23] Kumar, N., Suhr, B., Marschnig, S., Dietmaier, P., Marte, C., & Six, K. (2019). Micromechanical investigation of railway ballast behavior under cyclic loading in a box test using DEM: Effects of elastic layers and ballast types. Granular Matter, 21, 106. https://doi.org/10.1007/s10035-019-0956-9

[24] Verruijt, A. (2009). An introduction to soil dynamics (Vol. 24). Springer Science & Business Media.

[25] Acton, J. R., Squire P. T., (1985) Solving Equations with Physical Understanding, Adam Hilger Ltd, Bristol. 219 pp.